Molecules and Cells

WD Repeat Domain 1 Deficiency Inhibits Neointima Formation in Mice Carotid Artery by Modulation of Smooth Muscle Cell Migration and Proliferation

JiSheng Hu[1,2], ShangJing Pi[1,2], MingRui Xiong[1], ZhongYing Liu[1], Xia Huang[1], Ran An[1], TongCun Zhang[1,*], and BaiYin Yuan[1,*]

[1]Institute of Biology and Medicine, College of Life Science and Health, Wuhan University of Science and Technology, Hubei 430081, China, [2]These authors contributed equally to this work.
*Correspondence: yuanby@wust.edu.cn (BYY); zhangtongcun@wust.edu.cn (TCZ)
https://doi.org/10.14348/molcells.2020.0085
www.molcells.org

The migration, dedifferentiation, and proliferation of vascular smooth muscle cells (VSMCs) are responsible for intimal hyperplasia, but the mechanism of this process has not been elucidated. WD repeat domain 1 (WDR1) promotes actin-depolymerizing factor (ADF)/cofilin-mediated depolymerization of actin filaments (F-actin). The role of WDR1 in neointima formation and progression is still unknown. A model of intimal thickening was constructed by ligating the left common carotid artery in *Wdr1* deletion mice, and H&E staining showed that *Wdr1* deficiency significantly inhibits neointima formation. We also report that STAT3 promotes the proliferation and migration of VSMCs by directly promoting WDR1 transcription. Mechanistically, we clarified that WDR1 promotes the proliferation and migration of VSMCs and neointima formation is regulated by the activation of the JAK2/STAT3/WDR1 axis.

Keywords: migration, neointima formation, proliferation, vascular smooth muscle cells, WD repeat domain 1

INTRODUCTION

Vascular smooth muscle cells (VSMCs) are important participants in vascular pathological processes and are the predominant cell type in the arterial wall (Gomez and Owens, 2012; Ni et al., 2019; Owens et al., 2004). Proliferation and migration of VSMCs are key events in intimal hyperplasia (Allahverdian et al., 2018); these events are also prerequisites for diseases such as arteriosclerosis and restenosis after angioplasty (O'Brien et al., 2011; Xie et al., 2017). Under normal physiological conditions, VSMCs in the tunica media remain in a stationary state (Xie et al., 2017). In response to stimuli such as hypoxia and injury, VSMCs undergo a phenotypic transformation and proliferate (Intengan and Schiffrin, 2000; Xie et al., 2011). VSMCs also secrete extracellular matrix components, resulting in the intimal hyperplasia and vascular lumen stenosis that comprise neointima formation (Dzau et al., 2002; Jonasson et al., 1988; Marx and Marks, 2001; Weintraub, 2007).

Under physiological conditions, assembly and depolymerization of actin filaments coincide and maintain a balance, which is known as actin dynamics (Yuan et al., 2018). Cell motility and growth are inseparable from actin dynamics, and this process is regulated by various actin-binding proteins (Cooper and Schafer, 2000). Many factors are involved in depolymerization, such as actin-depolymerizing factor (ADF)/cofilin and WD repeat domain 1 (WDR1) (Bamburg, 1999; Cooper and Schafer, 2000). ADF/cofilin plays a crucial role in actin cleavage and depolymerization (Bravo-Cordero et

Received 3 April, 2020; revised 23 June, 2020; accepted 26 July, 2020; published online 19 August, 2020

eISSN: 0219-1032

al., 2013). WDR1 is a major cofactor for ADF/cofilin and promotes ADF/cofilin-mediated depolymerization of actin filaments (F-actin), thereby regulating the balance between actin depolymerization and assembly (Lee and Dominguez, 2010; Xu et al., 2015). WDR1-regulated actin dynamics directly affect cellular processes such as migration, cell-cell junction maintenance, and proliferation (Collazo et al., 2014; Lee et al., 2016). High expression of *Wdr1* in breast cancer cells can promote migration and proliferation (Lee et al., 2016). In previous work, we found that the deletion of *Wdr1* seriously affects the migration of adenocarcinoma human alveolar basal epithelial cells (Yuan et al., 2018). Deletion of *Wdr1* causes embryonic lethality (Hu et al., 2018), and loss of *Wdr1* in adult mouse heart tissue leads to cardiac hypertrophy (Huang et al., 2019). However, the role of WDR1 in smooth muscle cells and the development of intimal hyperplasia has yet to be elucidated.

Signal transducer and activator of transcription 3 (STAT3) is an important component of the Janus kinase (JAK/STAT) signaling pathway (Qi et al., 2016), which is involved in inflammation, as well as various cellular processes such as division, proliferation, drug resistance, and apoptosis (Fu et al., 2012; Hirano et al., 2000; Jackson and Ceresa, 2017; Limagne et al., 2017; Tripathi et al., 2017; Zulkifli et al., 2017). Binding of an extracellular signaling molecule (e.g., interleukin-6 [IL-6]) to its corresponding receptor on the cell surface induces the phosphorylation of JAK and its downstream transcription factor STATs (e.g., the IL-6/JAK/STAT3 pathway) (Chang et al., 2013; Johnson et al., 2018). Phosphorylated STAT3 forms homologous or heterologous dimers and then translocates to the nucleus (Souissi et al., 2011). STAT3 regulates the expression of downstream genes that are associated with growth, drug resistance, and inflammation, such as STK35, AKT2, and COX-2 (Kou et al., 2011; Qi et al., 2016; Wu et al., 2018). Studies have shown that STAT3 is crucial to neointima formation (Kovacic et al., 2010; Seki et al., 2000). However, the relationship between STAT3 and WDR1 and transcriptional regulation during vascular injury repair is unclear.

In this study, we propose a mechanism by which WDR1 regulates the proliferation of VSMCs and pathological intimal thickening. We demonstrated that after vascular injury, WDR1 promotes VSMC proliferation and migration, thereby promoting intimal thickening. After *Wdr1* knockout, neointima formation is inhibited. Finally, our results indicate that WDR1 promotes smooth muscle cell proliferation, migration, and intimal thickening via the JAK2/STAT3/WDR1pathway.

MATERIALS AND METHODS

Animal study and animal model

C57/BL6 male mice (7- to 8-weeks old) were obtained from the Model Animal Research Center of Nanjing University (Yuan et al., 2014). *Wdr*$^{f/+}$;ERT2Cre mice were housed and cared for by the Model Animal Research Center of Nanjing University. At two months of age, tamoxifen (T5648-5G; Sigma-Aldrich, USA) dissolved in oil (to induce Cre-mediated deletion) was administered to *Wdr1*$^{f/+}$;ERT2Cre mice and their *Wdr1*$^{f/+}$ littermates by intraperitoneal injection, as described previously. One week after the tamoxifen injection, a carotid artery ligation (CAL) was performed according to the protocol developed by Kumar (Kumar and Lindner, 1997). Briefly, five days after tamoxifen treatment, Avertin (400 mg/kg, T48402-25G; Sigma-Aldrich) was used to anesthetize the animal. A small neck incision was performed to separate the left common carotid artery, and it was ligated with 5-0 silk suture just below the carotid bifurcation. AG490 (cat No. S1143; Selleck Chemicals, USA), a specific inhibitor of JAK2, was dissolved in thermosensitive pluronic F-127 gel and administered to the ligation site to inhibit the activation of the JAK2/STAT3 pathway. Mice were sacrificed by cervical dislocation on different days after the ligation procedure. The carotid artery was perfused with phosphate-buffered saline (PBS), followed by 4% buffered formaldehyde through the left ventricle. Approximately 1.0 cm of the common carotid artery was then obtained from the proximal end of the ligation site. Cross-sections were obtained from the artery at 0.2 cm from the ligation site. The Institutional Animal Care and Use Committee (IACUC) of Wuhan University of Science and Technology approved all animal protocols used in this study (No. 2016CFB172).

Isolation of murine aortic vascular smooth muscle cells

Primary cultures of murine artery smooth muscle cells (MASMCs) were prepared from arteries. Briefly, aortas were isolated from 8 animals (*Wdr1*$^{f/f}$ or *Wdr1*$^{f/f}$;ERT2Cre) at 4 weeks, and the tissues were rinsed with PBS. The tissue was cut into pieces (1 mm^3) and digested with 1 mg/ml collagenase II for 1 h. Digestion was stopped by the addition of Dulbecco's modified Eagle's medium (DMEM) containing 10% fetal calf serum (FCS), and the cells released by the digestion were seeded into 6 cm dishes and cultured in DMEM with 10% FCS. Once cultures reached 80% to 90% confluence, they were trypsinized and seeded into plates and cells from the third to fifth passages are used for experiments.

Cell culture and drug treatment

Human aortic smooth muscle cells (HASMCs; National Infrastructure of Cell Line Resource, China) were grown in DMEM supplemented with 10% FCS and 1% penicillin/streptomycin at 37°C in a 5% CO_2 incubator. Cells were trypsinized at 80% to 90% confluence for experiments. HASMCs were seeded into 6-well plates, and when the cells reached 60% confluence, angiotensin II (Ang II, 200 nM; Sigma-Aldrich) and PDGF-BB (20 ng/ml; R&D Systems, USA) were added to the medium, and cells were collected at different times after treatment. Some HAVSMC cultures were stimulated with serum. For these cultures, cells were incubated in serum-free DMEM for 12 h and then treated with 10% fetal bovine serum. Cells were collected at various times after treatment.

Small interfering RNAs and DNA transfection

Small interfering RNA (siRNA) duplexes for silencing *Stat3* were designed using RNAi designer and synthesized by Genepharma. Lipofectamine RNAiMax (Invitrogen, USA) was used to transfect siRNAs, according to the manufacturer's protocol. HASMCs were seeded into 6-well plates (2×10^4 cells/well) and then transfected with siRNA. As a rescue experiment, at 12 h post-siRNA-transfection, the prepared

plasmid was mixed with an appropriate amount of the transfection reagent Lip 2000 (1 μg/well) and incubated at room temperature for 10 min. The transfection complex was then added dropwise to a 6-well plate. The sequence of the siRNA against *Stat3* is as follows: 5'-GCCCAACAUCUGCCUAGAUTT-3'.

Real-time PCR

RNA was extracted from HASMCs using TRIzol (Sigma-Aldrich). M-MLV reverse transcriptase (Vazyme Biotech, China) was used to synthesize cDNA. Real-time polymerase chain reaction (PCR) (Real-Time PCR Detection Systems; Bio-Rad, USA) was performed to assess the relative levels of mRNAs. Relative mRNA levels were normalized internally to GAPDH mRNA. Related primers are as follows: GAPDH (F): 5'-CATGTACGTTGCTATCCAGGC-3'; GAPDH (R): 5'-CTCCTTAATGTCACGCACGAT-3'; WDR1 (F): 5'-TTGTCAACTGTGTGCGATTCTC-3'; and WDR1 (R): 5'-GCTGTCGGGACTCCA ACTAA-3'.

Western blotting

Proteins were extracted from HASMCs, MASMCs, and murine artery tissues. Western blotting was performed as described previously (Hu et al., 2018). Primary antibodies included rabbit anti-WDR1 (cat No. 13676-1-AP, 1:1,000; Proteintech, USA), rabbit anti-STAT3 (cat No. 10253-2-AP, 1:1,000; Proteintech), rabbit anti-p-STAT3^{Tyr705} (cat No. 9415, 1:1,000; Cell Signaling Technology, USA), β-actin (cat No. AP0060, 1:5,000; Bioworld Technology, USA), rabbit anti-JAK2 (cat No. sc390539, 1:500; Santa Cruz Biotechnology, USA), and p-JAK2$^{Tyr1007/1008}$ (cat No. ab32102, 1:1,000; Abcam, UK). The membrane was washed using TBS-T and incubated with secondary antibody conjugated to horseradish peroxidase in 5% nonfat milk for 1 h at room temperature. Detection was carried out using a chemiluminescence detection kit (cat No.K-12045-D50; Advansta, USA).

Immunofluorescence staining

Arterial tissue samples were first washed with cold PBS and then fixed with 4% paraformaldehyde at 4°C. The samples were processed by successive incubation in (1) PBS for 20 min; (2) an ethanol series (70%, 85%, 95%, 95%, 100%, and 100%) for 1 h at room temperature; (3) butyl alcohol, three times for 30 min each at room temperature; and (4) fresh paraffin at 65°C, three times for 30 min each. The treated samples were embedded in paraffin, and 5-μm-thick sections were prepared. After the sections were dewaxed and rehydrated, immunofluorescence was performed according to standard protocols. Briefly, sections were incubated with mouse anti-α-SMA (cat No. ab32575, 1:200; Abcam) or rabbit anti-PH3 (cat No. 53348; Cell Signaling Technology) overnight at 4°C. After being washed with PBS three times, sections were incubated with Alexa Fluor 647-conjugated anti-mouse IgG (cat No. 4410S; Cell Signaling Technology) or Alexa Fluor 488-conjugated anti-rabbit IgG (cat No. 4416S; Cell Signaling Technology) for 30 min at room temperature. Slices were then stained with DAPI (1.0 mg/ml; Invitrogen) for 30 min before mounting. Images were captured with an Olympus confocal microscope (Olympus, Japan).

Histomorphometry

For immunohistochemistry (IHC), samples were prepared as described above, and sections were incubated with anti-WDR1 primary antibody and detected according to the IHC kit instructions (cat No. KIT-9707; Maixin Biotechnology, China). H&E staining was performed using standard protocols. H&E-stained arterial sections were analyzed by planimetry with ImageJ software.

Cell proliferation assay

Cell counting kit 8 (CCK-8) (cat No. A311-01; Vazyme Biotech) was used to detect cell proliferation between 0 h and 72 h according to the manufacturer's manual. Briefly, after tamoxifen-induced *Wdr1* knockout, MASMCs were seeded into 96-well plates. CCK-8 solution (10 μl) was added to each well, and the cells were incubated for an additional 2 h at 37°C. After 12 h of siRNA transfection, HAVSMCs were inoculated into 96-well plates. After 12 h, CCK8 reagent was added, and the cells were processed as described above. The absorbance of each well was measured at optical density at 450 nm (OD_{450}).

Cell migration analysis

MASMCs were seeded into 6-well plates for two days after induction with tamoxifen. After serum starvation for 24 h, a scratch was made using a sterile 200 μl pipette tip across each well, creating a cell-free area, based on the technique described by Yuan et al., and then 10 vol% fresh medium was added to the culture. Images were captured with a microscope at 0 h and 12 h. One day after transfection with siRNA, HASMCs were serum-starved for 12 h, and a scratch was made as described above.

Plasmid construction and dual-luciferase assays

The Phanta Super-Fidelity DNA Polymerase (cat No. P515-01; Vazyme Biotech) was used to perform a PCR to clone the murine *Wdr1* promoter. The 2000 bp *Wdr1* promoter was amplified by PCR with the following primers: F-5'-GCGTGCTAGCCCGGGCTCGAGTTACCCCAGCAGTCTTTGTAC-3' and R-5'-AACAGTACCGGAATGCCAAGCTTCGCGGAAGGCGGCGCCGG-3'.

The *Wdr1* promoter fragment was subcloned into the PGL3-Basic vector using the ClonExpress II One Step Cloning Kit (cat No. C112; Vazyme Biotech) to prepare the *Wdr1*-WT construct. The *Wdr1*-MUT construct was obtained by deleting the putative binding site of STAT3 using the Mut Express II Fast Mutagenesis Kit (cat No. C215-01; Vazyme Biotech) with the following primers: F-5'-TAGAAAGGTTATCGCTGTTATCTAAAACAAATAAGAAAGTC-3' and R-5'-AGAAGATAGTGTAGACTGTGACTTTCTTATTTGTTTTAGAT-3'.

Similarly, *Stat3* was cloned into the pCDNA3.1 vector using the following primers: F-5'-CCACCACACTGGACTAGTGGATCCATGGCTCAGTGGAACCAGC-3' and F-5'-GAGTTTTTGTTCGGGCCCAAGCTTTCACATGGGGGAGGTAGCA-3'.

The integrity and orientation of each insert were confirmed by sequencing. *Wdr1* promoter (*Wdr1*-WT, *Wdr1*-MUT), pCDNA3.1-STAT3, and pRL-TK (1,000 ng each construct) were then co-transfected into MASMCs cells. Luciferase ac-

tivity was measured using the Dual-Luciferase Reporter Assay System (cat No. E1910; Promega, USA) 48 h after transfection.

Chromatin immunoprecipitation (ChIP)

ChIP assays were performed using the SimpleChIP Enzymatic Chromatin IP Kit (cat No. 9002S; Cell Signaling Technology). MASMCs were treated with IL-6 (cat No. I9646; Sigma-Aldrich) for 30 min, and the cell lysate was used for immunoprecipitation with an antibody specific for the phosphorylated STAT3 (pSTAT3) protein (cat No. 9415; Cell Signaling Technology). PCR was performed on purified DNA from each sample using specific primers. The primer sequences used are listed below: F: 5'-TTACCCCAGCAGTCTTTGTACCAT-3' and R: 5'-AGCACTGTCCTAGGGATGTGCTAG-3'.

Flow cytometry

MASMCs were synchronized and induced with tamoxifen for two days as described above. Cells were fixed overnight in 75% ethanol at 4°C and stained for 10 min at room temperature with propidium iodide (50 mg/ml) and analyzed with a FACSCanto flow cytometer (BD Biosciences, USA). Cell-cycle detection was carried out by propidium iodide staining and fluorescence-activated cell sorting analysis. Each experiment was performed in triplicate.

Gelatin zymography

Mouse carotid arteries were harvested at various times post-injury, and the proteins were extracted with lysis buffer (50 mM Tris-HCl, pH 6.8; 10% glycerol; 1% SDS). Extracted proteins (10 mg) were loaded on 10% SDS-PAGE gels containing 1% gelatin to detect gelatinase activity. After washing in 2.5% Triton X-100, the gels were incubated overnight in buffer (10 mM $CaCl_2$, 0.01% NaN_3, and 50 mM Tris-HCl, pH 7.5). The obtained gels were stained with 0.2% Coomassie blue R-250 (Sigma-Aldrich) for 2 h and then destained with 10% acetic acid and 40% methanol.

Statistical analysis

Comparisons between two groups were performed using unpaired two-tailed Student's *t*-tests. Statistical analysis was performed by ANOVA/Dunnet's t-test for multiple group

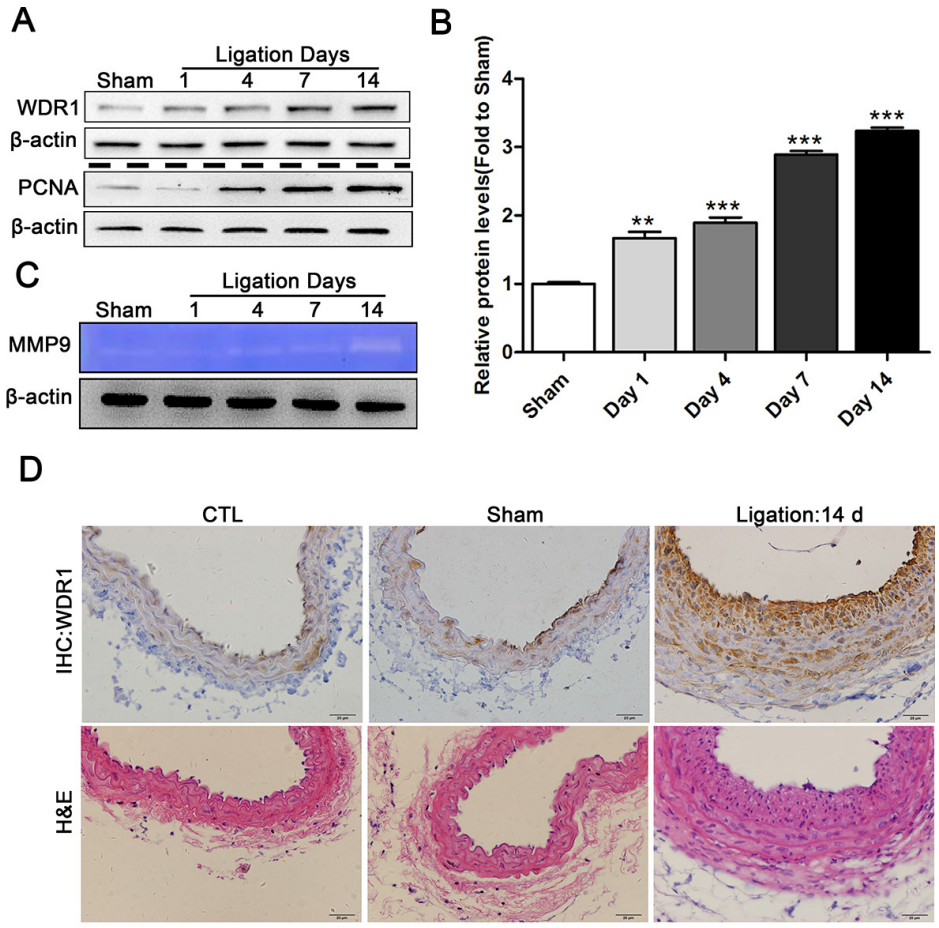

Fig. 1. WDR1 expression increases in the carotid artery after ligation. (A and B) Representative western blots of WDR1 and PCNA at 1, 4, 7, and 14 days after ligation, using the sham group as a control. $^{**}P < 0.01$; $^{***}P < 0.001$. (C) MMP9 activity as detected by gelatin zymography. (D) Immunohistochemical staining of vessels with anti-WDR1 antibody reveals WDR1 is localized primarily in the neointima. CTL, control group without any treatment. Scale bars = 20 μm.

comparisons. Data are expressed as the mean ± SEM. The threshold for statistical significance was set at $P < 0.05$. IBM SPSS Statistics (ver. 23.0; IBM, USA) was used for statistical analysis.

RESULTS

WDR1 expression after CAL is time-dependent

To investigate the effect of WDR1 on intimal thickening, we constructed a model of vascular injury in mice, and WDR1 levels were measured by western blot on different days post-injury (Figs. 1A and 1B). Furthermore, a gelatin zymography assay indicated that MMP9 activity in the ligation group was significantly increased compared with the sham group, indicating that injury facilitates SMC migration (Fig. 1C). To determine the localization and expression pattern of WDR1 in blood vessels, we performed immunohistochemical staining (Fig. 1D). WDR1 is primarily localized in the smooth muscle cells of blood vessels (Fig. 1D), and its level gradually increases as the number of days post-injury increases. These results suggest that WDR1 plays a key role in the repair of vascular injury.

WDR1 expression increases in proliferating SMCs

To investigate the potential effects of WDR1 in vascular biology and pathophysiology, we used the murine model of vascular injury for *in vivo* studies and cultured HASMCs for *in vitro* experiments. WDR1 increases significantly after 14 days of carotid artery injury (Fig. 1B). WDR1 levels in the injured and sham groups are not different on Day 1, and increase at 4, 7, and 14 days by western blot analysis (Fig. 1A). These results suggest that WDR1 in the vessel wall is upregulated in a time-dependent manner during neointima formation.

The response of WDR1 to various stimuli associated with vascular injury was investigated *in vitro*. WDR1 is significantly elevated at mRNA and protein levels after treatment with Ang II (200 nM) (Figs. 2A, 2D, and 2G). Similarly, the expression of WDR1 increases in response to serum (10% FCS) (Figs. 2B, 2E, and 2H) or platelet-derived growth factor-BB (PDGF-BB, 10 μg/L) (Figs. 2C, 2F, and 2I). These results indi-

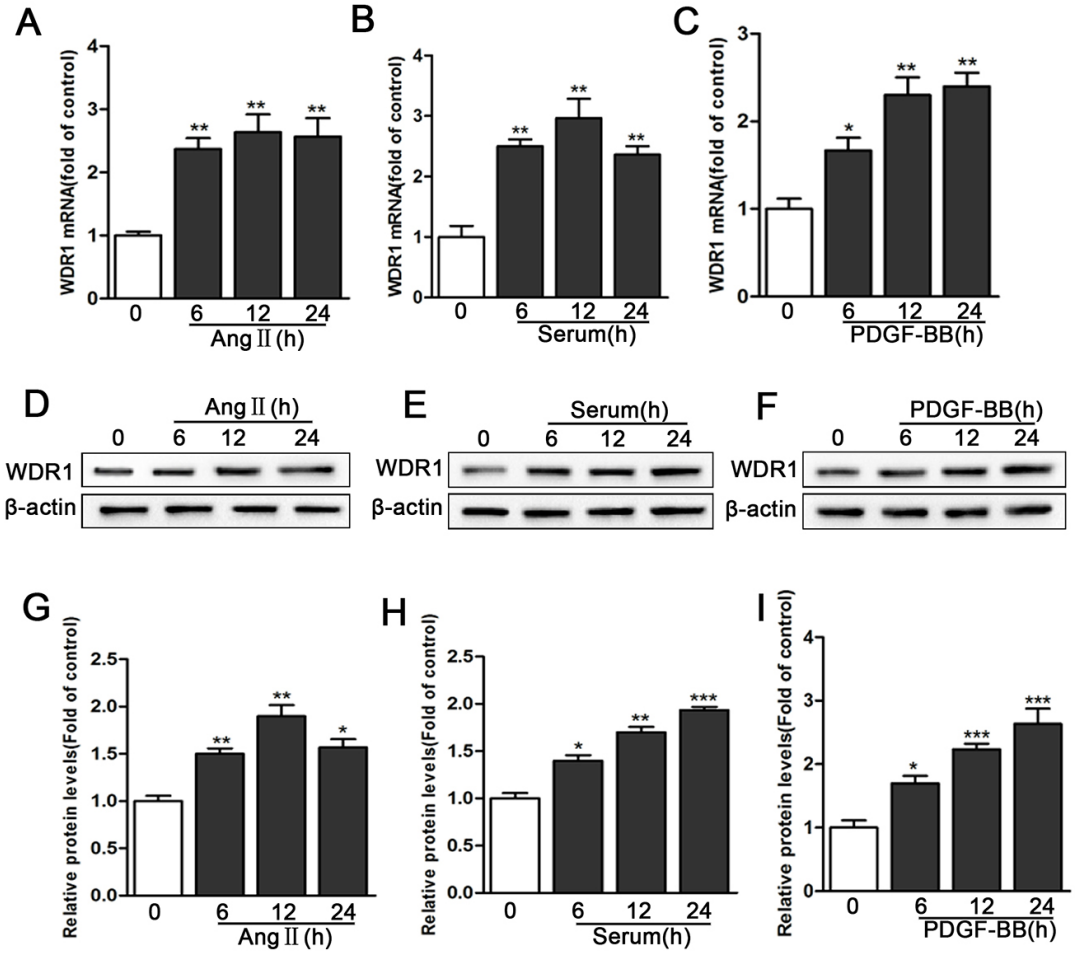

Fig. 2. WDR1 expression increases in proliferating HAVSMCs *in vitro*. (A-C) Real-time PCR data showing the mRNA levels of WDR1 in HASMCs treated with Ang II (200 nM), serum (10% FCS), and PDGF-BB (10 μg/L) at 6, 12, and 24 h (n = 3 per group). Representative western blots (D-F) and averaged data (G-I) showing WDR1 levels in HASMCs treated as in A-C. Data are expressed as mean ± SEM (n = 3 per group). $*P < 0.05$; $**P < 0.01$; $***P < 0.001$.

cate a close relationship between WDR1 and VSMC hyperplasia.

Wdr1 knockout inhibits neointima formation

Although WDR1 levels are increasing during neointima formation, it is unclear how WDR1 affects the process. Therefore, we performed CAL in *Wdr1*-deficient mice. Briefly, 10 mg/kg tamoxifen was administered daily to *Wdr1*$^{f/+}$;ERT2Cre and their *Wdr1*$^{f/+}$ littermates by intraperitoneal injection. After 5 days, western blot analysis was performed to detect the expression level of WDR1 in the carotid artery. WDR1 levels are significantly decreased after tamoxifen injection (Figs. 3A and 3B). After *Wdr1* knockout, left common CAL was performed, and the neointima formation was observed by

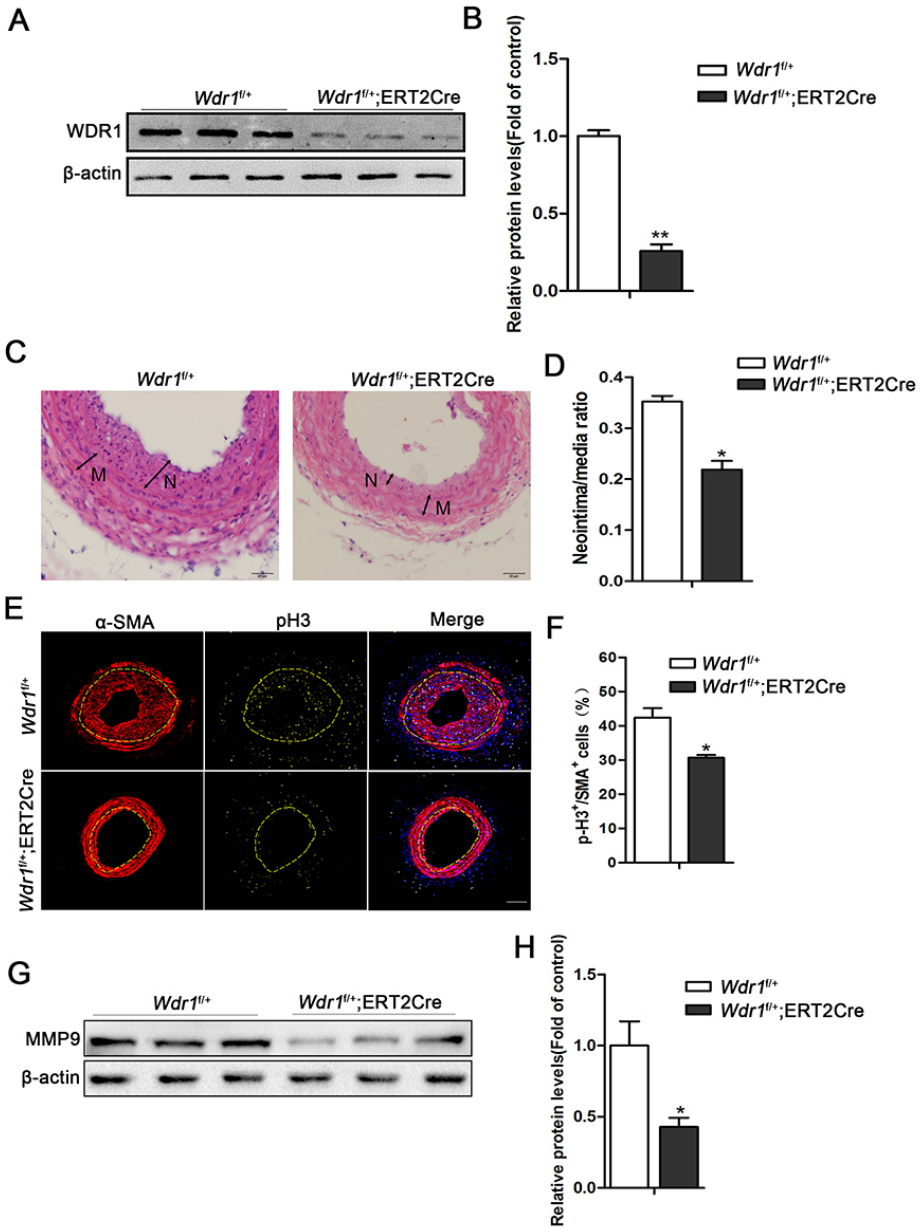

Fig. 3. Deletion of *Wdr1* inhibits neointima formation. (A and B) Western blot and averaged data showing the levels of WDR1 after 5 days of tamoxifen treatment, with male littermate *Wdr1*$^{f/+}$ mice as controls. (C and D) Representative photomicrographs of H&E staining and averaged data of neointima/media ratio in carotid arteries from *Wdr1*$^{f/+}$;ERT2Cre and *Wdr1*$^{f/+}$ control mice 14 days after CAL. N, neointima; M, media. Scale bars = 20 μm. (E and F) Immunofluorescence staining of α-SMA and PH3. The yellow dotted lines represent the boundary between the arterial tunica media and the intima. Scale bar = 50 μm. Statistical results show that the number of PH3-positive cells is significantly less in *Wdr1*$^{f/+}$;ERT2Cre mice than *Wdr1*$^{f/+}$ animals. (G and H) The level of MMP9 is significantly less in *Wdr1*$^{f/+}$;ERT2Cre mice after left common CAL compared with that in *Wdr1*$^{f/+}$ animals. Data are expressed as mean ± SEM (n = 4 per group). $*P < 0.05$; $**P < 0.01$.

H&E staining. As shown in the Figs. 3C and 3D, after *Wdr1* knockout, neointima formation is significantly inhibited (Figs. 3C and 3D). Neointima formation is primarily formed by the proliferation and migration of smooth muscle cells located in the middle layer of the arterial wall to the intima of the vessel. We performed immunofluorescence experiments and found that α-SMA accumulates significantly after *Wdr1* knockout. In contrast, the levels of phosphorylated histone H3 are significantly decreased (Figs. 3E and 3F). Compared with *Wdr1*$^{f/+}$ animals, MMP9 is decreased significantly after *Wdr1* knockdown (Fig. 3G and 3H). These data indicate that WDR1 may affect neointima formation by regulating the proliferation and migration of VSMCs. TUNEL assays were performed to rule out a possible effect of apoptosis on intimal formation, and the results show that the levels of apoptosis in *Wdr1*$^{f/+}$;ERT2Cre group and *Wdr1*$^{f/+}$ group cells are not statistically significant (data not shown). An effect of smooth muscle cells apoptosis induced by *Wdr1* knockout on neointima formation was excluded.

Wdr1 knockout inhibits proliferation and migration of smooth muscle cells

Knockdown of *Wdr1* in lung cancer cells and macrophages significantly reduced cell migration (Cervero et al., 2012; Yuan et al., 2018). To characterize the role of WDR1 in smooth muscle cells, we isolated primary murine aortic smooth muscle cells (MASMCs). Cells from *Wdr1*$^{f/f}$;ERT2Cre and *Wdr1*$^{f/f}$ mice were treated with tamoxifen (1 μM) for two days to induce Cre-mediated deletion (Figs. 4A and 4B), and then the proliferation and migration of MASMCs was measured. As shown in the Figs. 4C and 4D, after *Wdr1* knockout, the migration of smooth muscle cells decreases

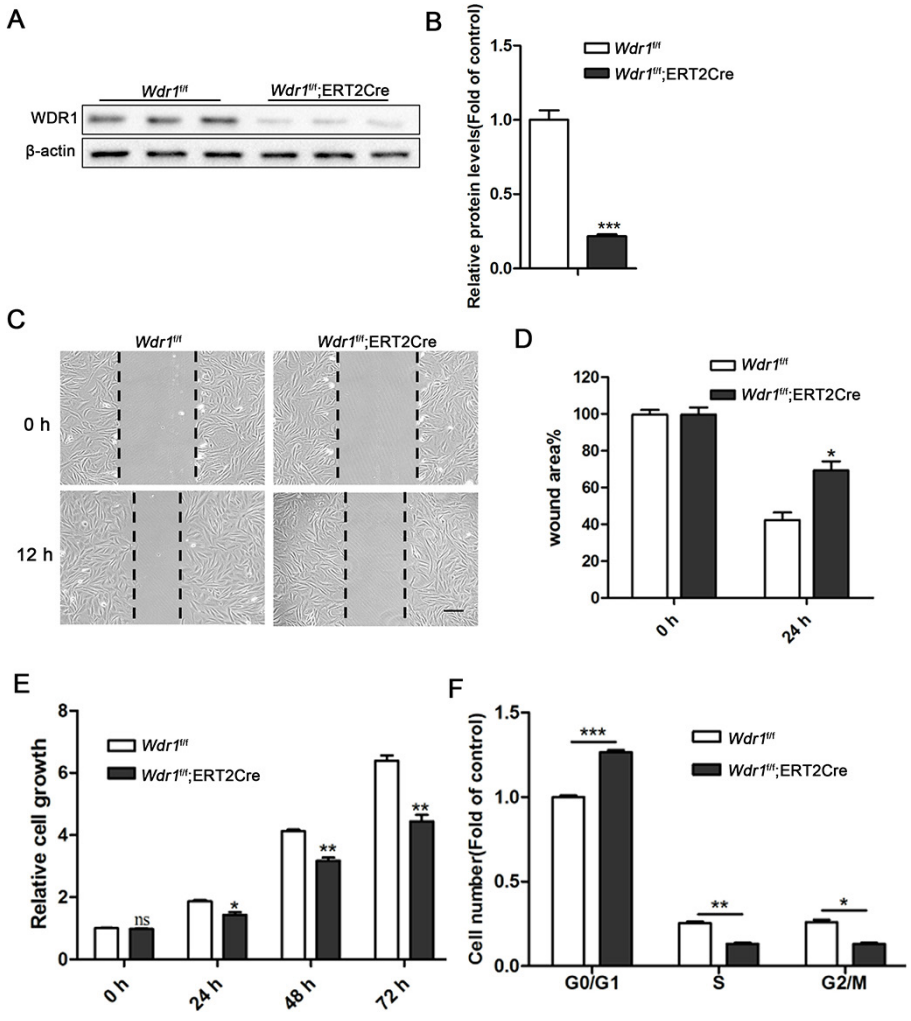

Fig. 4. Proliferation and migration are significantly inhibited in *Wdr1*-deficient smooth muscle cells. (A and B) Western blotting analysis and quantification are showing that levels of WDR1 in SMCs from *Wdr1*$^{f/f}$;ERT2Cre are less than those in SMCs from *Wdr1*$^{f/f}$ animals. (C and D) After tamoxifen-induced *Wdr1* knockout, wound-healing experiments and statistical results showing that SMCs from the *Wdr1*$^{f/f}$ group migrated faster than those *Wdr1*$^{f/f}$;ERT2Cre group (n = 3 per group). Scale bar = 200 μm. (E) CCK-8 assays of MASMCs treated with tamoxifen for 2 days (n = 9 per group). (F) Cell-cycle distribution in MASMCs in the absence of *Wdr1* (n = 3 per group). Data are expressed as mean ± SEM (n = 3 each). $*P < 0.05$; $**P < 0.01$; $***P < 0.001$; ns, not significant.

significantly (Figs. 4C and 4D). Similarly, the proliferation of MASMCs as measured by CCK-8 assay is significantly inhibited after *Wdr1* knockout (Fig. 4E). Because the cell cycle directly affects proliferation, we investigated the effect of *Wdr1* knockdown on cell proliferation in MASMCs by detecting the cell cycle (Fig. 4F). After *Wdr1* knockout, the percentage of proliferating cells in S and G2/M phases is decreased, and the percentage of cells in G0/G1 phase increases significantly (Fig. 4F). To rule out a possible effect of apoptosis, we performed TUNEL assays, and the results indicate that *Wdr1* knockout does not induce apoptosis (data not shown). In summary, *Wdr1* knockout in MASMCs inhibits cell migration and cell proliferation but does not induce apoptosis.

WDR1 promotes migration and proliferation of SMCs involved in the activation of the STAT3/WDR1 pathway

We investigated STAT3 activation by western blot in carotid artery tissue after ligation (Fig. 5A). After the injury, the levels of pSTAT3 (activated STAT3) increase and reach the highest level at 7 days post-ligation. The levels of WDR1 display a trend similar to those of pSTAT3 (Fig. 5A). These results suggest that STAT3 may regulate WDR1 to affect neointimal thickening. To test this hypothesis, we exposed cells to IL-6 and Ang II to simulate the release of cytokines following vascular injury. The proliferation and migration of SMCs are improved in response to IL-6 and Ang II (data not shown). As expected, pSTAT3 and WDR1 are elevated. In addition, we silenced *Wdr1* in HAVSMCs and found no changes in STAT3 and pSTAT3 levels (data not shown). It has been reported

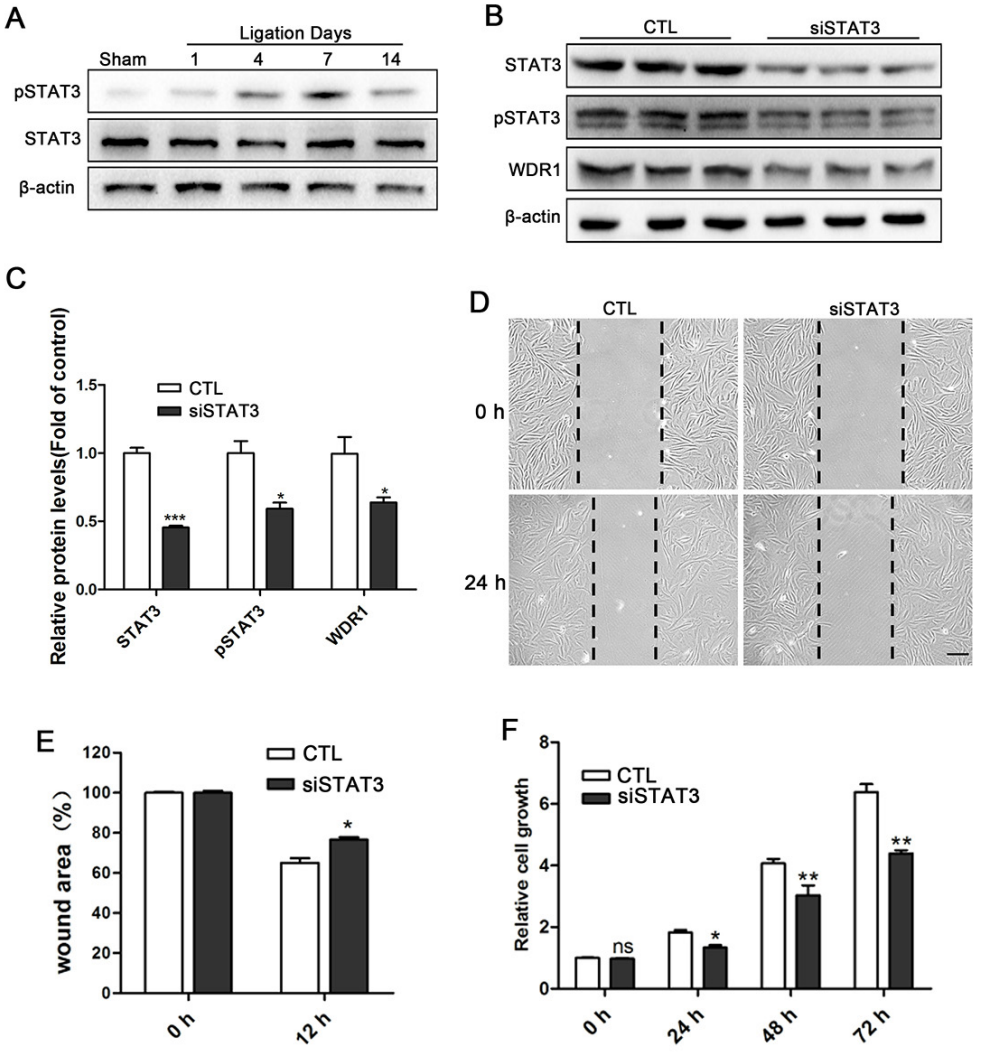

Fig. 5. *Stat3* knockdown inhibits proliferation and migration of HASMCs. (A) Western blot analysis showing changes in p-STAT3 after ligation of the left common carotid artery. (B and C) Western blot and analysis results indicate changes in WDR1 and p-STAT3 after HASMCS are transfected with *Stat3* siRNAs. (D and E) Representative images and wound areas from wound-healing assays in HASMCs transfected with *Stat3* siRNAs (n = 3 each). Scale bar = 200 μm. (F) CCK-8 assays of HASMCs transfected with *Stat3* siRNAs. $*P < 0.05$; $**P < 0.01$; $***P < 0.001$; ns, not significant.

that the cytoskeleton can affect the nuclear translocation of transcription factors. WDR is a cytoskeleton remodeling factor; however, it is unknown whether WDR1 affects nuclear trafficking of STAT3.

To study the interaction between WDR1 and STAT3, we used siRNA to decrease *Stat3* levels in HASMCs. The levels of WDR1 are significantly decreased after *Stat3* knockdown (Figs. 5B and 5C), and the proliferation and migration of HASMCs are significantly inhibited (Figs. 5D-5F). These results suggest that STAT3 affects SMC proliferation and migration by regulating WDR1. To test this hypothesis, we used overexpression of *Wdr1* to rescue the effect of Stat3 knockdown and performed cell migration and proliferation assays. Overexpression of *Wdr1* partially rescues the cell migration and proliferation inhibition that is observed in response to *Stat3* knockdown (Fig. 6).

STAT3 binds to the *Wdr1* promoter and facilitates transcription

Based on the results obtained above, we hypothesized that STAT3 binds directly to the *Wdr1* promoter and enhances its transcription in mice. We analyzed the 2 kb sequence up-

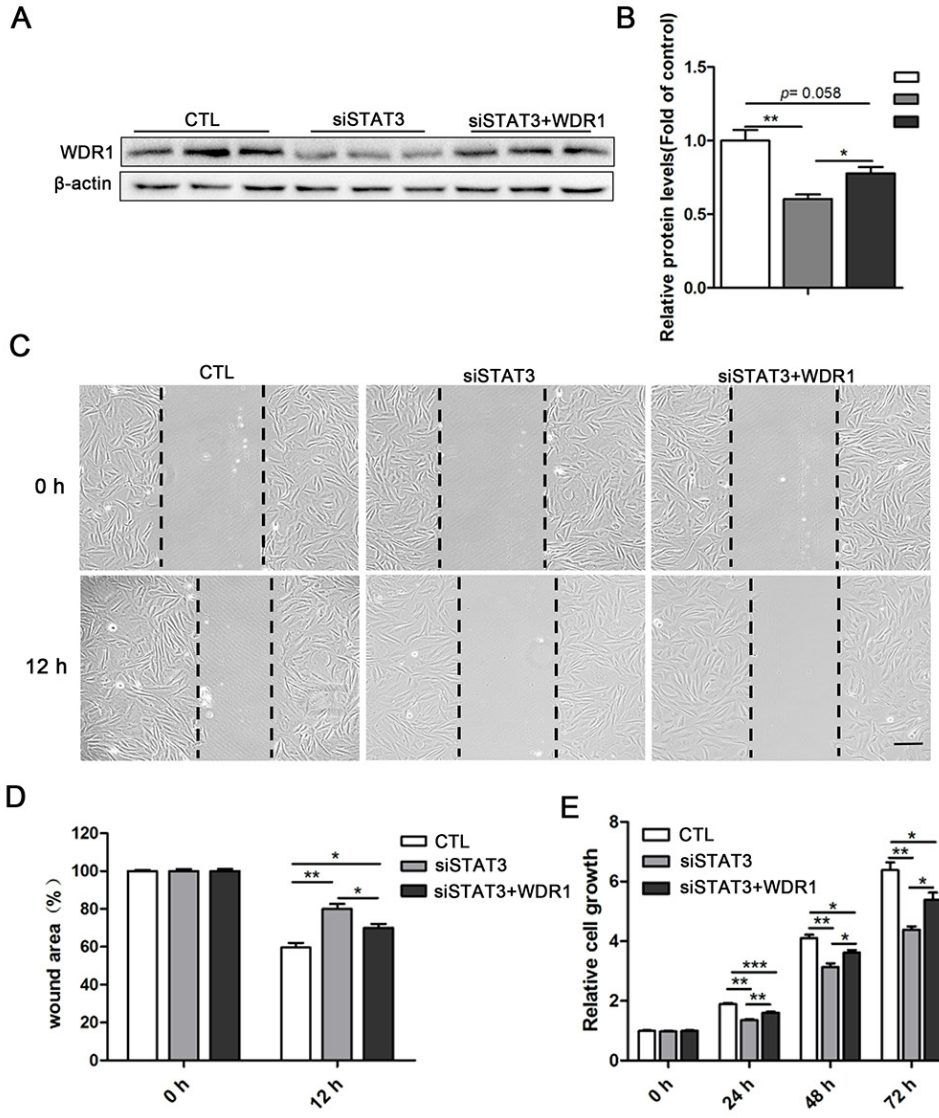

Fig. 6. Overexpression of *Wdr1* rescues impaired cell migration and proliferation in *Stat3* knockdown cells. (A and B) HASMCs were treated with *Stat3* siRNA and transfected with the pCDNA-WDR1 plasmid (siSTAT3+*Wdr1*). The transfection efficiency of WDR1 was determined by western blotting. Quantitation of the indicated proteins to the corresponding control is also shown. (C and D) Representative images and averaged data from wound-healing assays in *Stat3*-siRNA-treated HASMCs show that forced overexpression of *Wdr1* rescues the decrease in cell migration caused by *Stat3* knockdown (n = 3 per group). Scale bar = 200 μm. (E) CCK-8 assay in HASMCs treated with *Stat3* siRNA and transfected with the pCDNA-WDR1 plasmid (n = 3 per group). $*P < 0.05$; $**P < 0.01$; $***P < 0.001$.

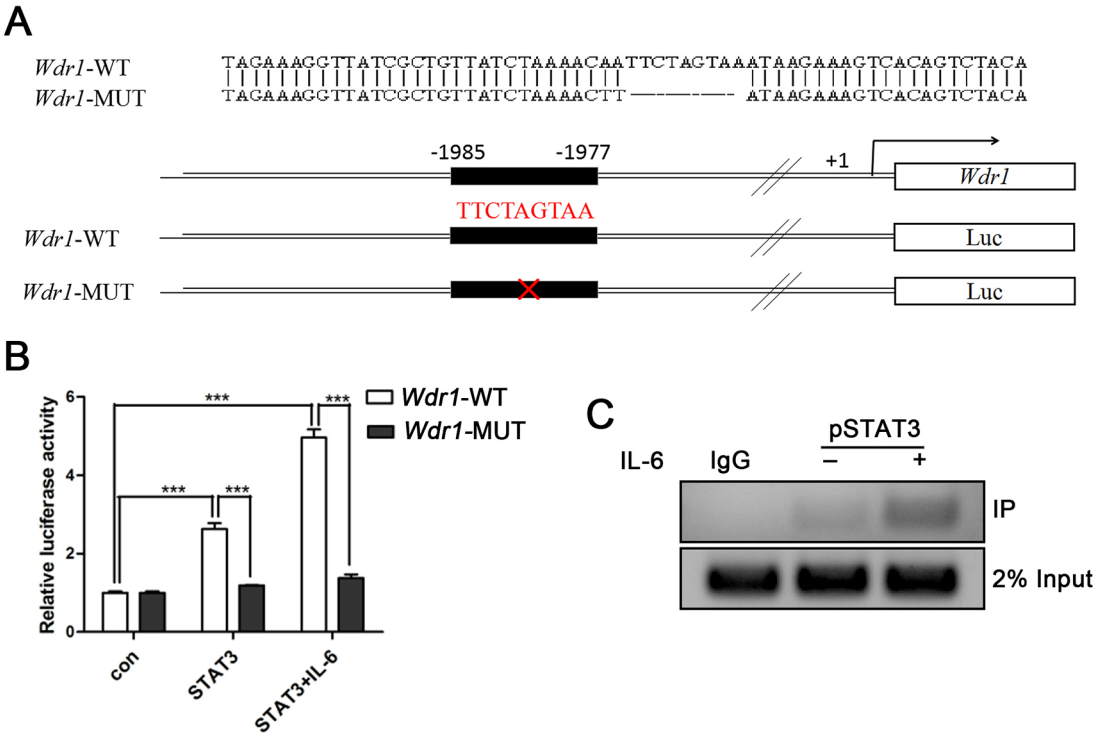

Fig. 7. STAT3 binds directly to the *Wdr1* promoter region. (A) Schematic representation of the *Wdr1* promoter. The black box indicates the expected binding region of STAT3. The arrow represents the transcription start site. A red cross indicates the deletion of the binding site. (B) Luciferase assay to measure pSTAT3 binding to the *Wdr1* promoter. Dual-luciferase assays were performed in the MASMCs cells co-transfected with pRL-TK (Renilla activity for normalization) and the wild-type 2 kb upstream sequence of the *Wdr1* gene (*Wdr1*-WT) or the putative binding site-deletion mutant (*Wdr1*-MUT) and PCDNA-STAT3 plasmid. ***$P < 0.001$. (C) ChIP with anti-pSTAT3. MASMCs were serum-starved for 12 h and then treated with IL-6 for 30 min. ChIP assays were performed with a p-STAT3 (Tyr 705) antibody. STAT3 binding to the *Wdr1* promoter was examined using PCR with the primers described above (n = 6 per group).

stream of the mouse *Wdr1* gene and predicted the binding site of STAT3 using the transcription factor binding prediction network (JASPAR). The putative binding site of STAT3 is located in the −1985 to −1977 region of the *Wdr1* promoter (Fig. 7A). The wild type (*Wdr1*-WT) and mutant (*Wdr1*-MUT) promoter sequences were cloned into a pGL3-Basic vector. pRL-TK and pCDNA 3.1-STAT3 were co-transfected into MASMCs with *Wdr1*-WT or *Wdr1*-MUT, and luciferase activity was detected. The *Wdr1*-MUT plasmid was obtained by deleting the putative STAT3 binding site (Fig. 7A). The luciferase activity of cells transfected with *Wdr1*-WT is approximately 3-fold higher than that of control cells transfected with the pGL3-Basic vector (Fig. 7B). In addition, the luciferase activity of cells treated with IL-6 was approximately 5-fold higher than that of the control group (Fig. 7B). The results show that there is no difference in luciferase activity between the cells transfected with *Wdr1*-MUT plasmid and control cells (Fig. 7B). ChIP was performed with an anti-pSTAT3 antibody to confirm the binding of pSTAT3 to the putative site in the *Wdr1* promoter. Compared to untreated cells, the binding of STAT3 to the *Wdr1* promoter is significantly increased in MASMCs treated with IL-6 (Fig. 7C).

Inhibition of JAK2/STAT3 pathway reduces WDR1 expression and neointima formation

WDR1-mediated SMCs migration and proliferation require the activation of STAT3. To elucidate additional details about this result, we conducted *in vivo* experiments in mice. Briefly, ligation was performed at the bifurcation of the left common carotid artery in C57/BL6 adult male mice, and the artery was immediately covered with 50 μl of 25% thermosensitive pluronic F-127 gel containing AG490 (1 mg/ml) or vehicle (DMSO). At 7 days post-ligation, western blotting was performed to detect STAT3 activation and WDR1 levels in the left common carotid artery. Similarly, at 14 days post-ligation, H&E staining was performed to detect the neointima formation after AG490 treatment. As expected, western blot analysis shows that STAT3 activation is significantly inhibited by AG490 relative to the control group, and the expression of WDR1 is also significantly decreased (Figs. 8A and 8B). H&E staining shows that intimal thickening is also blocked (Figs. 8C-8E). These results demonstrate that WDR1-mediated neointima formation requires the activation of STAT3.

DISCUSSION

Intimal thickening caused by abnormal proliferation of SMCs

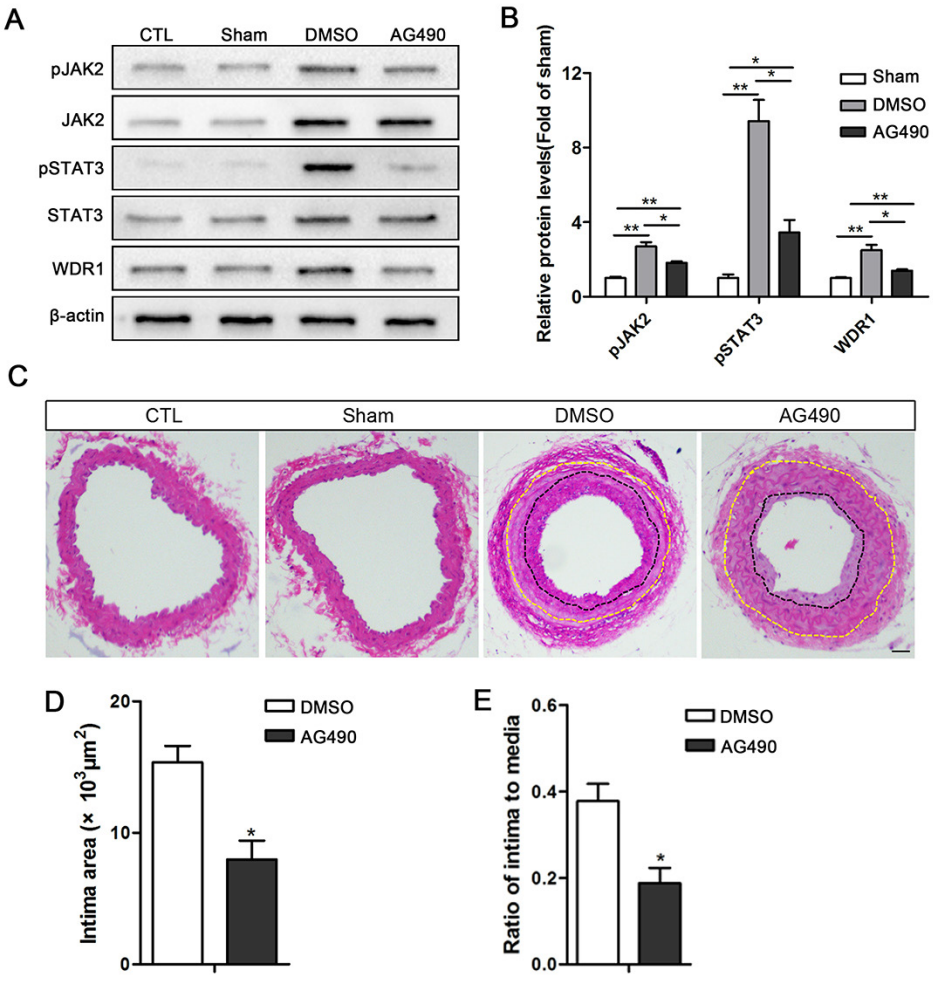

Fig. 8. Inhibition of the JAK2/STAT3 pathway *in vivo* inhibits neointima formation. (A and B) The activation of JAK2/STAT3 in the ligation group treated with AG490 on at 7 days post-ligation is downregulated. The level of WDR1 decreases significantly. (C-E) Morphometry analysis of CAL and AG490 treatment at 14 days post-ligation. The neointimal area and neointima/media ratio are quantified. The black dotted lines represent the boundary between the arterial tunica media and the neointima; the yellow dotted lines indicate the external elastic lamina (n = 6 per group). Scale bar = 50 μm. $*P < 0.05$; $**P < 0.01$.

is associated with a variety of diseases (Xie et al., 2017). The proliferation and migration of SMCs caused by endogenous and exogenous factors are crucial steps in the repair of vascular injury (O'Brien et al., 2011; Zhang et al., 2014). However, our understanding of the underlying mechanisms for these responses in SMCs is poor.

WDR1 acts as a cofactor of cofilin for actin depolymerization and plays a vital role in cellular processes, such as proliferation and migration (Yuan et al., 2018). However, the function of WDR1 in SMCs is not understood. Therefore, we constructed *Wdr1* knockout mice and successfully constructed an arterial injury model. We also isolated arterial smooth muscle cells from *Wdr1* knockout mice for *in vitro* experiments. We observed that the expression of WDR1 was elevated during the repair of vascular injury (Fig. 1). However, after *Wdr1* knockout in the artery, intimal thickening was blocked (Fig. 3). Furthermore, *Wdr1* knockout in MASMCs significantly inhibited cell proliferation and migration (Fig. 4). These results suggest that WDR1 is associated with the repair of vascular injury.

The process of vascular remodeling after vascular injury is divided into four stages (Schwartz et al., 1995; Seki et al., 2000). The first stage occurs within a few days of injury when the proliferation of the medial VSMCs is maximal. The second stage involves the migration of SMCs to the intima, starting between day 4 and 5. The third stage involves the continuous proliferation of SMCs in the neointima. During the fourth stage, extracellular matrix components are secreted and deposited. Inflammation, cytokine production, and VSMC proliferation are key aspects of vascular repair, and inflammation, and cytokines are active in the first phase of vascular remodeling. Unfortunately, endometrial remodeling elicits a series of negative results. Decreased lumen diameter causes thrombosis, which in turn leads to serious cardiovascular diseases such as myocardial and cerebral infarctions.

JAK and STAT proteins transmit intracellular signals in a variety of cell types in response to various cytokines (Li et al., 2019). Previous reports have shown that JAK2/STAT3 is responsive to angiotensin II type 1 receptor and is activated after tyrosine phosphorylation in rat smooth muscle cells (Marrero et al., 1997; Seki et al., 2000; Watanabe et al., 2004). Activated STAT3 translocates to the nucleus after homologous or heterologous dimer formation and binds to cis-inducing elements in the nucleus, leading to transcriptional activation of early growth response genes (Li et al., 2019). When SMCs were treated with the JAK2-specific inhibitor AG490, proliferation was significantly inhibited, suggesting that the JAK2/STAT3 pathway is vital to smooth muscle cell

proliferation.

In this study, we investigated the role of the STAT3-WDR1 axis in neointima formation after vascular injury. JAK2/STAT3 was induced in the tunica media and intima, beginning at the first stage and peaking in the second and third stages. We found that levels of STAT3 and WDR1 increased synergistically in a certain period of time during arterial injury repair. Therefore, we hypothesized that STAT3 regulates the transcription of *Wdr1* to strengthen neointima formation. To test this hypothesis, we knocked down *Stat3* in HASMCs. Intriguingly, our data indicate that *Stat3* deficiency inhibits proliferation and migration of HASMCS cells, and the expression of *Wdr1* is also dramatically reduced (Fig. 5). Consistent with expectations, in response to overexpression of *Wdr1*, the inhibition of proliferation and migration caused by STAT3 deletion in SMCs was partially attenuated (Fig. 6). This result agrees with previous reports that STAT3 not only regulates *Wdr1* to promote thickening of the intima, but STAT3 also works through other pathways (Zhang et al., 2018). As a transcription factor, STAT3 affects multiple downstream processes, such as cell proliferation and drug resistance (Kou et al., 2011; Tripathi et al., 2017). Through bioinformatics analysis, we found that there is a specific binding site for STAT3 on the *Wdr1* promoter, and we confirmed it by chIP assays (Fig. 7). STAT3 promotes *Wdr1* transcription by binding to the *Wdr1* promoter in MASMCs. Finally, we demonstrated that activated STAT3 is involved in WDR1-mediated intimal thickening by blocking the JAK2/STAT3 pathway *in vivo* (Fig. 8).

We successfully combined *Wdr1* conditional knockout mice with a vascular injury model and reported for the first time that WDR1 regulates the proliferation and migration of VSMCs cells. STAT3 was identified as an upstream regulator of *Wdr1* by bioinformatics. We have verified *in vitro* that STAT3 promotes *Wdr1* transcription by molecular biological methods, but no further verification has been conducted *in vivo* at a histological level. The *in vivo* situation is complicated. WDR1 is as a cytoskeleton depolymerization factor. Whether WDR1 regulates biological processes in smooth muscle cells through ADFcofilin-mediated actin dynamics remains to be explored. Nevertheless, we demonstrate that WDR1-mediated SMC proliferation, migration, and intimal thickening require STAT3 activation (Fig. 9). The JAK2/STAT3/

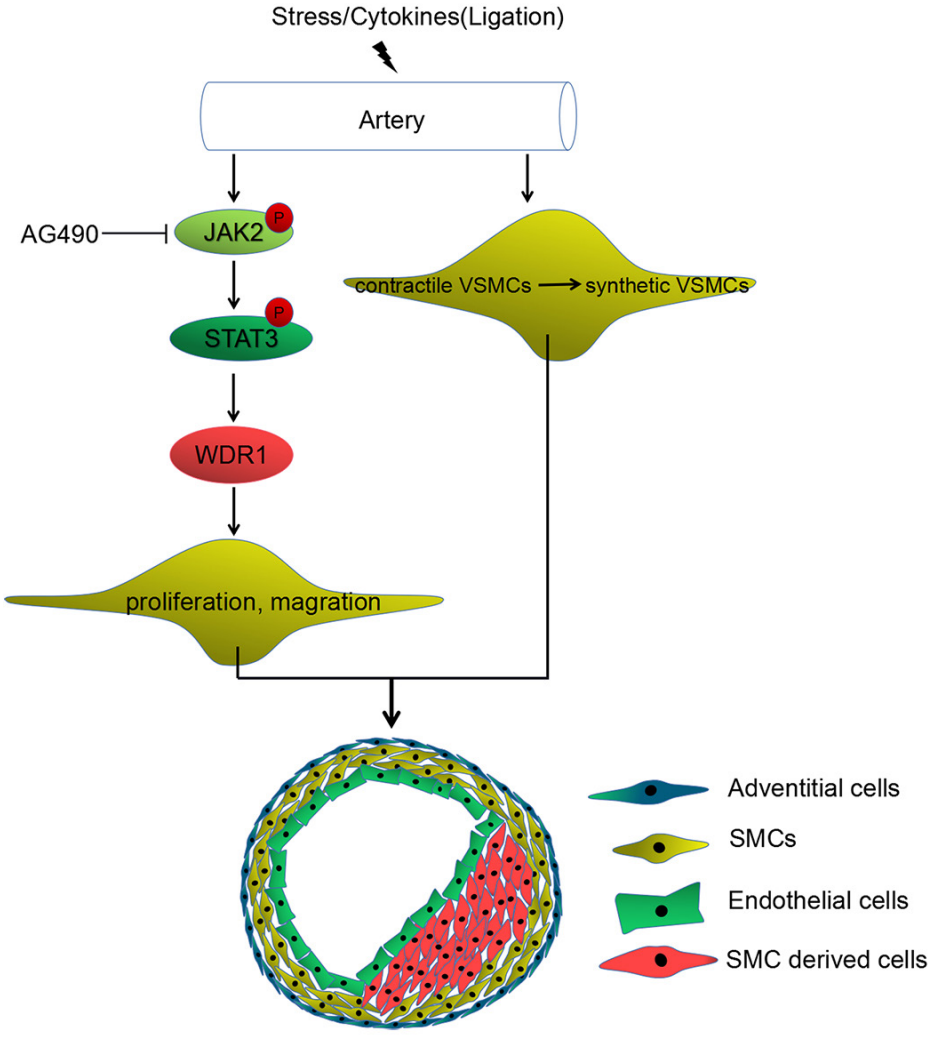

Fig. 9. Schematic diagram of how the STAT3/WDR1 signaling axis promotes intimal thickening. When the artery is exposed to stimuli (e.g., external force, hypoxia, or inflammation), cytokines that activate the JAK2/STAT3 pathway are released. Activated STAT3 translocates to the nucleus, where it directly increases the transcriptional activity and subsequent expression of WDR1. Elevated levels of WDR1 enhance the proliferation and migration of smooth muscle cells. Smooth muscle cell phenotype conversion and the enhancement of migration and proliferation capacities are key factors that promote the formation of vascular intima.

WDR1 pathway is crucial to vascular pathology and may have therapeutic implications for atherosclerosis, post-stent restenosis, and other vascular proliferative diseases. Knockdown of *Wdr1* blocks the translocation of myocardin-related transcription factor-A (MRTF-A) by inhibiting the expression of importin β (Xiang et al., 2017). Nuclear translocation of STAT3 is affected by many factors, such as nuclear transport protein importin and small GTP proteases (Cimica et al., 2011). The actin cytoskeleton plays an essential role in nuclear trafficking (Minakhina et al., 2005). Whether WDR1 is involved in the nuclear translocation of STAT3 remains unclear. The regulation of STAT3 nuclear translocation by WDR1 will be one direction of our future research; another course will be to provide a more comprehensive and flexible strategy for solving the problem of vascular restenosis.

ACKNOWLEDGMENTS

This work was supported by the National Natural Science Foundation of China (No. 31701266).

AUTHOR CONTRIBUTIONS

J.S.H. and B.Y.Y. conceived and designed the study. J.S.H., S.J.P., M.R.X., X.H., Z.Y.L., and R.A. performed the experiments. J.S.H. wrote the paper. J.S.H., B.Y.Y., S.J.P., M.R.X., and T.C.Z. reviewed and edited the manuscript. All authors read and approved the manuscript.

CONFLICT OF INTEREST

The authors have no potential conflicts of interest to disclose.

ORCID

JiSheng Hu	https://orcid.org/0000-0002-8330-4485
ShangJing Pi	https://orcid.org/0000-0003-4410-0217
MingRui Xiong	https://orcid.org/0000-0001-8131-9758
ZhongYing Liu	https://orcid.org/0000-0003-0413-9280
Xia Huang	https://orcid.org/0000-0001-9668-0503
Ran An	https://orcid.org/0000-0002-2417-0552
TongCun Zhang	https://orcid.org/0000-0001-5350-2993
BaiYin Yuan	https://orcid.org/0000-0002-6266-6241

REFERENCES

Allahverdian, S., Chaabane, C., Boukais, K., Francis, G.A., and Bochaton-Piallat, M.L. (2018). Smooth muscle cell fate and plasticity in atherosclerosis. Cardiovasc. Res. *114*, 540-550.

Bamburg, J.R. (1999). Proteins of the ADF/cofilin family: essential regulators of actin dynamics. Annu. Rev. Cell Dev. Biol. *15*, 185-230.

Bravo-Cordero, J.J., Magalhaes, M.A., Eddy, R.J., Hodgson, L., and Condeelis, J. (2013). Functions of cofilin in cell locomotion and invasion. Nat. Rev. Mol. Cell Biol. *14*, 405-415.

Cervero, P., Himmel, M., Kruger, M., and Linder, S. (2012). Proteomic analysis of podosome fractions from macrophages reveals similarities to spreading initiation centres. Eur. J. Cell Biol. *91*, 908-922.

Chang, Q., Bournazou, E., Sansone, P., Berishaj, M., Gao, S.P., Daly, L., Wels, J., Theilen, T., Granitto, S., Zhang, X., et al. (2013). The IL-6/JAK/Stat3 feed-forward loop drives tumorigenesis and metastasis. Neoplasia *15*, 848-862.

Cimica, V., Chen, H.C., Iyer, J.K., and Reich, N.C. (2011). Dynamics of the STAT3 transcription factor: nuclear import dependent on Ran and importin-beta1. PLoS One *6*, e20188.

Collazo, J., Zhu, B., Larkin, S., Martin, S.K., Pu, H., Horbinski, C., Koochekpour, S., and Kyprianou, N. (2014). Cofilin drives cell-invasive and metastatic responses to TGF-beta in prostate cancer. Cancer Res. *74*, 2362-2373.

Cooper, J.A. and Schafer, D.A. (2000). Control of actin assembly and disassembly at filament ends. Curr. Opin. Cell Biol. *12*, 97-103.

Dzau, V.J., Braun-Dullaeus, R.C., and Sedding, D.G. (2002). Vascular proliferation and atherosclerosis: new perspectives and therapeutic strategies. Nat. Med. *8*, 1249-1256.

Fu, Y., Zhao, Y., Liu, Y., Zhu, Y., Chi, J., Hu, J., Zhang, X., and Yin, X. (2012). Adenovirus-mediated tissue factor pathway inhibitor gene transfer induces apoptosis by blocking the phosphorylation of JAK-2/STAT-3 pathway in vascular smooth muscle cells. Cell. Signal. *24*, 1909-1917.

Gomez, D. and Owens, G.K. (2012). Smooth muscle cell phenotypic switching in atherosclerosis. Cardiovasc. Res. *95*, 156-164.

Hirano, T., Ishihara, K., and Hibi, M. (2000). Roles of STAT3 in mediating the cell growth, differentiation and survival signals relayed through the IL-6 family of cytokine receptors. Oncogene *19*, 2548-2556.

Hu, J., Shi, Y., Xia, M., Liu, Z., Zhang, R., Luo, H., Zhang, T., Yang, Z., and Yuan, B. (2018). WDR1-regulated actin dynamics is required for outflow tract and right ventricle development. Dev. Biol. *438*, 124-137.

Huang, X., Li, Z., Hu, J., Yang, Z., Liu, Z., Zhang, T., Zhang, C., and Yuan, B. (2019). Knockout of Wdr1 results in cardiac hypertrophy and impaired cardiac function in adult mouse heart. Gene *697*, 40-47.

Intengan, H.D. and Schiffrin, E.L. (2000). Structure and mechanical properties of resistance arteries in hypertension: role of adhesion molecules and extracellular matrix determinants. Hypertension *36*, 312-318.

Jackson, N.M. and Ceresa, B.P. (2017). EGFR-mediated apoptosis via STAT3. Exp. Cell Res. *356*, 93-103.

Johnson, D.E., O'Keefe, R.A., and Grandis, J.R. (2018). Targeting the IL-6/JAK/STAT3 signalling axis in cancer. Nat. Rev. Clin. Oncol. *15*, 234-248.

Jonasson, L., Holm, J., and Hansson, G.K. (1988). Cyclosporin A inhibits smooth muscle proliferation in the vascular response to injury. Proc. Natl. Acad. Sci. U. S. A. *85*, 2303-2306.

Kou, X., Qi, S., Dai, W., Luo, L., and Yin, Z. (2011). Arctigenin inhibits lipopolysaccharide-induced iNOS expression in RAW264.7 cells through suppressing JAK-STAT signal pathway. Int. Immunopharmacol. *11*, 1095-1102.

Kovacic, J.C., Gupta, R., Lee, A.C., Ma, M., Fang, F., Tolbert, C.N., Walts, A.D., Beltran, L.E., San, H., Chen, G., et al. (2010). Stat3-dependent acute Rantes production in vascular smooth muscle cells modulates inflammation following arterial injury in mice. J. Clin. Invest. *120*, 303-314.

Kumar, A. and Lindner, V. (1997). Remodeling with neointima formation in the mouse carotid artery after cessation of blood flow. Arterioscler. Thromb. Vasc. Biol. *17*, 2238-2244.

Lee, J.H., Kim, J.E., Kim, B.G., Han, H.H., Kang, S., and Cho, N.H. (2016). STAT3-induced WDR1 overexpression promotes breast cancer cell migration. Cell. Signal. *28*, 1753-1760.

Lee, S.H. and Dominguez, R. (2010). Regulation of actin cytoskeleton dynamics in cells. Mol. Cells *29*, 311-325.

Li, Y.L., Ding, K., Hu, X., Wu, L.W., Zhou, D.M., Rao, M.J., Lin, N.M., and Zhang, C. (2019). DYRK1A inhibition suppresses STAT3/EGFR/Met signalling and sensitizes EGFR wild-type NSCLC cells to AZD9291. J. Cell. Mol. Med. *23*, 7427-7437.

Limagne, E., Thibaudin, M., Euvrard, R., Berger, H., Chalons, P., Vegan, F., Humblin, E., Boidot, R., Rebe, C., Derangere, V., et al. (2017). Sirtuin-1 activation controls tumor growth by impeding Th17 differentiation via STAT3 deacetylation. Cell Rep. *19*, 746-759.

Marrero, M.B., Schieffer, B., Li, B., Sun, J., Harp, J.B., and Ling, B.N. (1997). Role of Janus kinase/signal transducer and activator of transcription and

mitogen-activated protein kinase cascades in angiotensin Ⅱ- and platelet-derived growth factor-induced vascular smooth muscle cell proliferation. J. Biol. Chem. *272*, 24684-24690.

Marx, S.O. and Marks, A.R. (2001). Bench to bedside: the development of rapamycin and its application to stent restenosis. Circulation *104*, 852-855.

Minakhina, S., Myers, R., Druzhinina, M., and Steward, R. (2005). Crosstalk between the actin cytoskeleton and Ran-mediated nuclear transport. BMC Cell Biol. *6*, 32.

Ni, Z., Deng, J., Potter, C.M.F., Nowak, W.N., Gu, W., Zhang, Z., Chen, T., Chen, Q., Hu, Y., Zhou, B., et al. (2019). Recipient c-Kit lineage cells repopulate smooth muscle cells of transplant arteriosclerosis in mouse models. Circ. Res. *125*, 223-241.

O'Brien, E.R., Ma, X., Simard, T., Pourdjabbar, A., and Hibbert, B. (2011). Pathogenesis of neointima formation following vascular injury. Cardiovasc. Hematol. Disord. Drug Targets *11*, 30-39.

Owens, G.K., Kumar, M.S., and Wamhoff, B.R. (2004). Molecular regulation of vascular smooth muscle cell differentiation in development and disease. Physiol. Rev. *84*, 767-801.

Qi, Z., Qi, S., Ling, L., Lv, J., and Feng, Z. (2016). Salidroside attenuates inflammatory response via suppressing JAK2-STAT3 pathway activation and preventing STAT3 transfer into nucleus. Int. Immunopharmacol. *35*, 265-271.

Schwartz, S.M., deBlois, D., and O'Brien, E.R. (1995). The intima. Soil for atherosclerosis and restenosis. Circ. Res. *77*, 445-465.

Seki, Y., Kai, H., Shibata, R., Nagata, T., Yasukawa, H., Yoshimura, A., and Imaizumi, T. (2000). Role of the JAK/STAT pathway in rat carotid artery remodeling after vascular injury. Circ. Res. *87*, 12-18.

Souissi, I., Najjar, I., Ah-Koon, L., Schischmanoff, P.O., Lesage, D., Le Coquil, S., Roger, C., Dusanter-Fourt, I., Varin-Blank, N., Cao, A., et al. (2011). A STAT3-decoy oligonucleotide induces cell death in a human colorectal carcinoma cell line by blocking nuclear transfer of STAT3 and STAT3-bound NF-kappaB. BMC Cell Biol. *12*, 14.

Tripathi, S.K., Chen, Z., Larjo, A., Kanduri, K., Nousiainen, K., Aijo, T., Ricano-Ponce, I., Hrdlickova, B., Tuomela, S., Laajala, E., et al. (2017). Genome-wide analysis of STAT3-mediated transcription during early human Th17 cell differentiation. Cell Rep. *19*, 1888-1901.

Watanabe, S., Mu, W., Kahn, A., Jing, N., Li, J.H., Lan, H.Y., Nakagawa, T., Ohashi, R., and Johnson, R.J. (2004). Role of JAK/STAT pathway in IL-6-induced activation of vascular smooth muscle cells. Am. J. Nephrol. *24*, 387-392.

Weintraub, W.S. (2007). The pathophysiology and burden of restenosis. Am. J. Cardiol. *100*, 3K-9K.

Wu, Z., Liu, J., Hu, S., Zhu, Y., and Li, S. (2018). Serine/threonine kinase *35*, a target gene of STAT*3*, regulates the proliferation and apoptosis of osteosarcoma cells. Cell. Physiol. Biochem. *45*, 808-818.

Xiang, Y., Liao, X.H., Yao, A., Qin, H., Fan, L.J., Li, J.P., Hu, P., Li, H., Guo, W., Li, J.Y., et al. (2017). MRTF-A-miR-206-WDR1 form feedback loop to regulate breast cancer cell migration. Exp. Cell Res. *359*, 394-404.

Xie, C., Ritchie, R.P., Huang, H., Zhang, J., and Chen, Y.E. (2011). Smooth muscle cell differentiation in vitro: models and underlying molecular mechanisms. Arterioscler. Thromb. Vasc. Biol. *31*, 1485-1494.

Xie, N., Chen, M., Dai, R., Zhang, Y., Zhao, H., Song, Z., Zhang, L., Li, Z., Feng, Y., Gao, H., et al. (2017). SRSF1 promotes vascular smooth muscle cell proliferation through a Delta133p53/EGR1/KLF5 pathway. Nat. Commun. *8*, 16016.

Xu, J., Wan, P., Wang, M., Zhang, J., Gao, X., Hu, B., Han, J., Chen, L., Sun, K., Wu, J., et al. (2015). AIP1-mediated actin disassembly is required for postnatal germ cell migration and spermatogonial stem cell niche establishment. Cell Death Dis. *6*, e1818.

Yuan, B., Wan, P., Chu, D., Nie, J., Cao, Y., Luo, W., Lu, S., Chen, J., and Yang, Z. (2014). A cardiomyocyte-specific Wdr1 knockout demonstrates essential functional roles for actin disassembly during myocardial growth and maintenance in mice. Am. J. Pathol. *184*, 1967-1980.

Yuan, B., Zhang, R., Hu, J., Liu, Z., Yang, C., Zhang, T., and Zhang, C. (2018). WDR1 promotes cell growth and migration and contributes to malignant phenotypes of non-small cell lung cancer through ADF/cofilin-mediated actin dynamics. Int. J. Biol. Sci. *14*, 1067-1080.

Zhang, L., Shao, J., Zhou, Y., Chen, H., Qi, H., Wang, Y., Chen, L., Zhu, Y., Zhang, M., Chen, L., et al. (2018). Inhibition of PDGF-BB-induced proliferation and migration in VSMCs by proanthocyanidin A2: Involvement of KDR and Jak-2/STAT-3/cPLA2 signaling pathways. Biomed. Pharmacother. *98*, 847-855.

Zhang, S.M., Zhu, L.H., Chen, H.Z., Zhang, R., Zhang, P., Jiang, D.S., Gao, L., Tian, S., Wang, L., Zhang, Y., et al. (2014). Interferon regulatory factor 9 is critical for neointima formation following vascular injury. Nat. Commun. *5*, 5160.

Zulkifli, A.A., Tan, F.H., Putoczki, T.L., Stylli, S.S., and Luwor, R.B. (2017). STAT3 signaling mediates tumour resistance to EGFR targeted therapeutics. Mol. Cell. Endocrinol. *451*, 15-23.